ELSEVIER

Journal of Organometallic Chemistry 549 (1997) 127–137

Journal of Organometallic Chemistry

# Organometallic complexes for nonlinear optics. X. [1] Molecular quadratic and cubic hyperpolarizabilities of systematically varied (cyclopentadienyl)bis(phosphine)ruthenium σ-arylacetylides: X-ray crystal structure of Ru((*E*)-4,4′-C≡$CC_6H_4CH$=$CHC_6H_4NO_2$)($PPh_3$)$_2$($\eta$-$C_5H_5$)

Ian R. Whittall [a], Marie P. Cifuentes [a], Mark G. Humphrey [a,*], Barry Luther-Davies [b], Marek Samoc [b], Stephan Houbrechts [c], André Persoons [c], Graham A. Heath [d], David C.R. Hockless [d]

[a] *Department of Chemistry, Australian National University, Canberra, ACT 0200, Australia*

[b] *Australian Photonics Cooperative Research Centre, Laser Physics Centre, Research School of Physical Sciences and Engineering, Australian National University, Canberra, ACT 0200, Australia*

[c] *Centre for Research on Molecular Electronics and Photonics, Laboratory of Chemical and Biological Dynamics, University of Leuven, Celestijnenlaan 200D, Leuven B-3001, Belgium*

[d] *Research School of Chemistry, Australian National University, Canberra, ACT 0200, Australia*

Received 7 May 1997; received in revised form 2 July 1997

**Abstract**

The complexes Ru(4,4′-C≡$CC_6H_4NO_2$)($PPh_3$)$_2$($\eta$-$C_5H_5$) and Ru(4,4′-C≡$CC_6H_4$C≡$CC_6H_4NO_2$)($PPh_3$)$_2$($\eta$-$C_5H_5$) have been prepared and the latter structurally characterized; they belong to a series of organometallic donor–bridge–acceptor compounds containing (cyclopentadienyl)bis(phosphine)ruthenium(II) centres as donors, conjugated arylacetylide bridges, and nitro acceptor groups. Electrochemical data for the series of complexes Ru(C≡CR)($PR'_3$)$_2$($\eta$-$C_5H_5$) (R=Ph, 4-$C_6H_4NO_2$, R′=Ph, Me; R=4,4′-$C_6H_4C_6H_4NO_2$, (*E*)-4,4′-$C_6H_4CH$=$CHC_6H_4NO_2$, 4,4′-$C_6H_4$C≡$CC_6H_4NO_2$, 4,4′-$C_6H_4N$=$CHC_6H_4NO_2$, R′=Ph) are consistent with an $Ru^{II/III}$ couple whose oxidation potentials vary strongly with chain-lengthening from one-ring to two-ring acetylide ligand, but show little variation with changes at the bridging unit of the two-ring acetylide ligand. The molecular quadratic and cubic optical nonlinearities of the series of complexes have been determined by hyper-Rayleigh scattering (HRS) and Z-scan techniques, respectively. Molecular first hyperpolarizabilities by HRS at 1064 nm are dispersively enhanced; experimental and two-level corrected data suggest an increase in nonlinearity on chain-lengthening of the bridge, in proceeding from $C_6H_4$ to $C_6H_4C_6H_4$ and then $C_6H_4$C≡$CC_6H_4$ and $C_6H_4CH$=$CHC_6H_4$, a general trend that is reproduced by semiempirical ZINDO computations. Cubic hyperpolarizabilities by Z-scan at 800 nm are negative for complexes with nitro acceptor groups, probably a result of two-photon dispersion, with absolute values (up to $850 \times 10^{-36}$ esu) large for small organometallic complexes; as with quadratic nonlinearities, cubic nonlinearities increase substantially on bridge lengthening, with little variation on phosphine substitution. © 1997 Elsevier Science S.A.

*Keywords:* Acetylide; Alkynyl; Susceptibility; Ruthenium; Nonlinear optics; X-ray structure

## 1. Introduction

Investigations of the nonlinear optical (NLO) responses of materials have recently focused on organometallic complexes [1–5]; a combination of fast response time, low-lying intense MLCT or LMCT transitions, and the potential of variable oxidation state, *d*-electron count and ligand environment in tuning NLO performance suggests that organometallics or metal-organics may have an advantageous combination of properties. Despite this, few investigations correlating quadratic or cubic NLO response with systematically varying structural elements have been promulgated [2]. Metal σ-acetylide complexes have the metal in the

* Corresponding author. Tel.: +61-26249-2927; fax: +61-26249-0760; e-mail: mark.humphrey@anu.edu.au.

[1] For Part IX, see I.R. Whittall, M.G. Humphrey, M. Samoc, B. Luther-Davies, Angew. Chem., Int. Ed. Engl., 36 (1997) 370.


*PII* S0022-328X(97)00411-7

same plane as the extended $\pi$-system of the ligand; strong charge transfer transitions between the metal and acetylide ligand may result in large optical nonlinearities. In addition, metal $\sigma$-acetylide complexes are frequently more oxidatively stable and thermally robust than complexes containing other $\sigma$-bound carbon ligands, factors which are important considerations for potential applications in devices. We have recently been studying the NLO performance of systematically varied metal $\sigma$-acetylide complexes [6–14] and report herein synthetic details for the 'extended chromophore' acetylides $Ru(C \equiv CR)(PPh_3)_2(\eta\text{-}C_5H_5)$ (R=4,4'-$C_6H_4C_6H_4NO_2$, 4,4'-$C_6H_4C \equiv CC_6H_4NO_2$), their experimentally-derived quadratic optical nonlinearities at 1064 nm by hyper-Rayleigh scattering (HRS), their computationally-derived molecular first hyperpolarizabilities at 1907 nm from ZINDO, an X-ray structural study of the yne-linked complex $Ru(4,4'\text{-}C \equiv CC_6H_4C \equiv CC_6H_4NO_2)(PPh_3)_2(\eta\text{-}C_5H_5)$, and a comprehensive investigation of the electrochemical behaviour and cubic optical nonlinearities at 800 nm by Z-scan and degenerate four-wave mixing (DFWM) of the series $Ru(C \equiv CR)(PR'_3)_2(\eta\text{-}C_5H_5)$ (R = Ph, 4-$C_6H_4NO_2$, R' = Ph, Me; R = 4,4'-$C_6H_4C_6H_4NO_2$, (*E*)-4,4'-$C_6H_4CH{=}CHC_6H_4NO_2$, 4,4'-$C_6H_4C \equiv CC_6H_4NO_2$, 4,4'-$C_6H_4N{=}CHC_6H_4NO_2$, R' = Ph); some of the molecular second hyperpolarizabilities have been communicated previously [8].

## 2. Results and discussion

### 2.1. Syntheses of terminal alkynes and $\sigma$-acetylide complexes

The acetylene 4,4'-$HC \equiv CC_6H_4C_6H_4NO_2$ (**1**) was prepared from 4,4'-bromonitrobiphenyl, the latter obtained from commercially available 4-nitrobiphenyl by bromination following the method of Le Fèvre and Turner [15]; subsequent ethynylation of the bromo compound by palladium(II)/copper(I)-catalyzed coupling with trimethylsilylacetylene, followed by removal of the trimethylsilyl protecting group with base, afforded the product (Scheme 1). The acetylene 4,4'-$HC \equiv CC_6H_4C \equiv CC_6H_4NO_2$ (**2**) was prepared by a similar palladium(II)/copper(I) coupling of 4-iodonitrobenzene with an excess of diethynylbenzene (the product of an analogous coupling of trimethylsilylacetylene with diiodobenzene and deprotection with base) [16] (Scheme 2). Both new terminal alkynes were characterized by a combination of IR, $^1H$, and $^{13}C$ NMR spectra and satisfactory microanalyses. The ruthenium acetylide synthetic methodology successfully utilized for the preparation of $Ru(4,4'\text{-}C \equiv CC_6H_4C_6H_4NO_2)(PPh_3)_2(\eta\text{-}C_5H_5)$ (**7**) and $Ru(4,4'\text{-}C \equiv CC_6H_4C \equiv CC_6H_4NO_2)(PPh_3)_2(\eta\text{-}C_5H_5)$ (**9**) (Scheme 3) has been described in detail elsewhere [6,7,17].

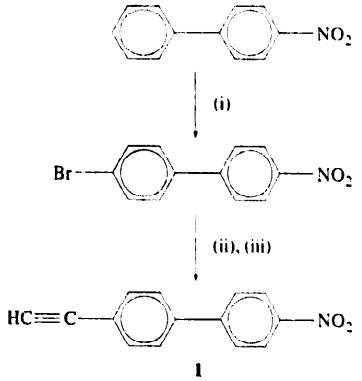


1

Scheme 1. (i) $Br_2$, $CH_3COOH$; (ii) $Me_3SiC \equiv CH$, $PdCl_2(PPh_3)_2$, CuI, $NEt_3$; (iii) $K_2CO_3$, MeOH.

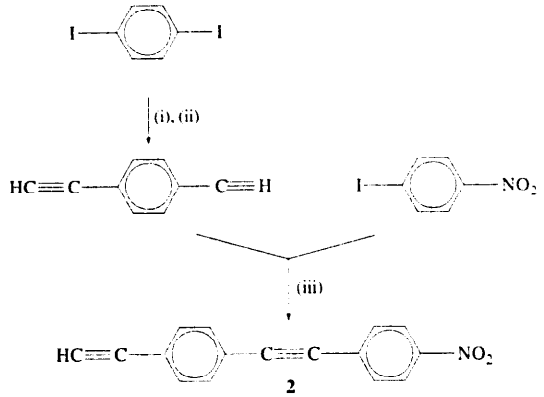


2

Scheme 2. (i) $Me_3SiC \equiv CH$, $PdCl_2(PPh_3)_2$, CuI, $NEt_3$; (ii) $K_2CO_3$, MeOH; (iii) $PdCl_2(PPh_3)_2$, CuI, $NEt_3$.

Complexes **7** and **9** were characterized by IR, $^1H$, $^{13}C$ and $^{31}P$ NMR spectroscopies and satisfactory microanalyses. Characteristic $\nu(C \equiv C)$ in the solution IR spectra show some solvent dependence [2074 (cyclohexane), 2068 ($CH_2Cl_2$) $cm^{-1}$, **7**; 2070, 2065 $cm^{-1}$, **9**]; as with the related complexes $Ru((E)\text{-}4,4'\text{-}C \equiv CC_6H_4X{=}CHC_6H_4NO_2)(PR_3)_2(\eta\text{-}C_5H_5)$ (X = CH, N; R = Ph, Me) [7], the shift to lower energy in the more polar solvent is consistent with increased stabilization of a charge-separated vinylidene contributor [Ru-C $\equiv$ C-Ar $\leftrightarrow$ $Ru^+{=}C{=}C{=}Ar^-$]. The $^1H$ (4.33 ppm, **7**;

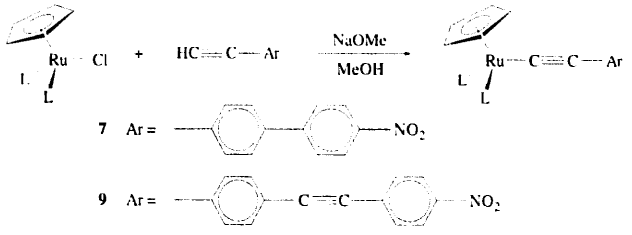


Scheme 3.

Table 1
Important bond lengths (Å) and angles (°) for complex **9**

| | | | |
|---|---|---|---|
| Ru–P(1) | 2.300(1) | C(6)–C(7) | 1.383(7) |
| Ru–P(2) | 2.283(1) | C(6)–C(15) | 1.449(6) |
| Ru–($\eta$-$C_5H_5$) | 2.216(5) | C(7)–C(8) | 1.361(6) |
| | 2.213(5) | C(9)–C(10) | 1.389(7) |
| | 2.230(5) | C(9)–C(14) | 1.372(7) |
| | 2.221(5) | C(9)–C(16) | 1.433(6) |
| | 2.231(5) | C(10)–C(11) | 1.398(8) |
| Ru–C(1) | 1.986(4) | C(11)–C(12) | 1.366(8) |
| C(1)–C(2) | 1.211(6) | C(12)–C(13) | 1.333(8) |
| C(2)–C(3) | 1.440(6) | C(12)–N(1) | 1.480(8) |
| C(3)–C(4) | 1.379(6) | C(13)–C(14) | 1.373(7) |
| C(3)–C(8) | 1.387(6) | C(15)–C(16) | 1.167(6) |
| C(4)–C(5) | 1.385(6) | N(1)–O(1) | 1.251(8) |
| C(5)–C(6) | 1.391(6) | N(1)–O(2) | 1.148(9) |
| Ru–C(1)–C(2) | 174.1(4) | C(6)–C(15)–C(16) | 174.3(6) |
| P(1)–Ru–P(2) | 99.25(4) | C(9)–C(16)–C(15) | 174.2(6) |
| C(1)–Ru–P(1) | 91.2(1) | C(12)–N(1)–O(1) | 112.2(8) |
| C(1)–Ru–P(2) | 89.8(1) | C(12)–N(1)–O(2) | 119.7(9) |
| C(1)–C(2)–C(3) | 175.1(5) | O(1)–N(1)–O(2) | 128.1(9) |

4.32 ppm, **9**) and $^{13}C$ NMR spectra (85.3 ppm, **7**; 85.3 ppm, **9**) contain resonances for the cyclopentadienyl groups which, as we have found previously [7], do not vary with subtle changes to the acetylide ligand. The metal-bound acetylide $\alpha$-carbon (124.2 ppm, **7**; 126.6 ppm, **9**) shows a small variation (2.4 ppm) on acetylide modification.

### 2.2. X-ray structural study of 9

We have completed an X-ray diffraction study of **9** to compare it with the data from cognate (acetylide)ruthenium complexes we have crystallographically characterized previously [6,7], and to provide reliable input data for the semiempirical computational work detailed below. Important bond lengths and angles for **9** are given in Table 1 and data from related complexes displayed in Table 2. An ORTEP plot of **9** is displayed in Fig. 1.

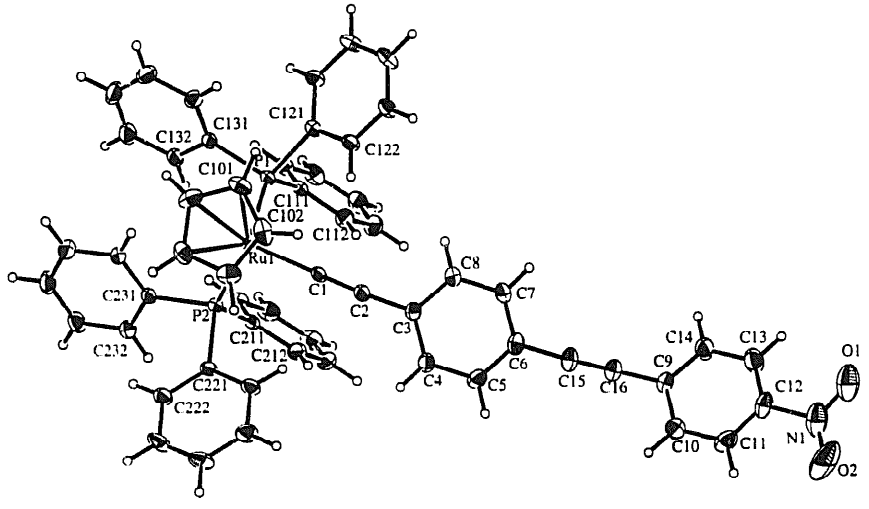


Fig. 1. Molecular structure and atomic labeling scheme for **9**. 20% thermal ellipsoids are shown for the non-hydrogen atoms; hydrogen atoms have arbitrary radii.

Table 2
Selected structural data for (cyclopentadienyl)bis(phosphine)ruthenium acetylide complexes

| | Ru–C(1) | C(1)–C(2) | C(2)–C(3) | Ru–C(1)–C(2) | C(1)–C(2)–C(3) |
|---|---|---|---|---|---|
| Ru(4,4′-C ≡ $CC_6H_4C$ ≡ $CC_6H_4NO_2$)($PPh_3$)$_2$($\eta^5$-$C_5H_5$) (**9**)[a] | 1.986(4) | 1.211(6) | 1.440(6) | 174.1(4) | 175.1(5) |
| Ru(C ≡ CPh)($PMe_3$)$_2$($\eta^5$-$C_5H_5$) (**4b**)[b] | 1.989(7) | 1.224(10) | 1.430(9) | 177.7(6) | 174.5(7) |
| Ru(4-C ≡ $CC_6H_4NO_2$)($PMe_3$)$_2$($\eta^5$-$C_5H_5$) (**6b**)[b] | 1.99(2) | 1.23(2) | 1.43(3) | 178(2) | 177(3) |
| [Ru(C = CFc)($PMe_3$)$_2$($\eta^5$-$C_5H_5$)][$PF_6$][c] | 1.99(2) | 1.19(3) | 1.38(3) | 173(2) | 178(3) |
| Ru(4-C ≡ $CC_6H_4NO_2$)($PPh_3$)$_2$($\eta^5$-$C_5H_5$) (**6a**)[b] | 1.994(5) | 1.202(8) | 1.432(7) | 175.9(4) | 175.0(9) |
| Ru((*E*)-4,4′-C ≡ $CC_6H_4CH$=$CHC_6H_4NO_2$)($PPh_3$)$_2$($\eta^5$-$C_5H_5$) (**8**)[d] | 2.008(6) | 1.199(7) | 1.438(8) | 174.2(6) | 177.6(7) |
| Ru(C ≡ CPh)(dppe)($\eta^5$-$C_5H_5$)[e] | 2.009(3) | 1.204(5) | 1.444(5) | 178.1(3) | 176.3(4) |
| Ru(C ≡ CPh)($PPh_3$)$_2$($\eta^5$-$C_5H_5$) (**4a**)[f] | 2.016(3) | 1.215(4) | 1.456(4) | 178.0(2) | 171.9(3) |
| Ru(C ≡ CPh)($PPh_3$)$_2$($\eta^5$-$C_5H_5$)(**4a**)[g] | 2.017(5) | 1.214(7) | 1.462(8) | 177.7(4) | 170.6(5) |
| Ru(C ≡ CPh)($Ph_2CHMeCHMePPh_2$)($\eta^5$-$C_5H_5$)[g] | 2.038(7) | 1.172(9) | [h] | [h] | [h] |

[a]This work. [b]Ref. [6]. [c]Ref. [18]. [d]Ref. [7]. [e]Ref. [19]. [f]Ref. [20]. [g]Ref. [21]. [h]Not reported.

Ru–P distances for **9** (2.300(1), 2.283(1) Å) are comparable to Ru(4-C ≡ $CC_6H_4NO_2$)($PPh_3$)$_2$($\eta$-$C_5H_5$) (**6a**) (2.297(2), 2.301(2) Å) [6] and Ru((*E*)-4,4′-C ≡ $CC_6H_4CH{=}CHC_6H_4NO_2$)($PPh_3$)$_2$($\eta$-$C_5H_5$) (**8**) (2.292(2), 2.280(2) Å) [7], and substantially longer than those in Ru(C ≡ CPh)($PPh_3$)$_2$($\eta$-$C_5H_5$) (**4a**) (2.229(3), 2.228(3) Å) [19]; with no significant steric differences between these complexes, substantial electronic differences deriving from the presence of the strong acceptor acetylide ligands can be considered responsible for Ru–P bond-length variations. The Ru–C(1) vector in **9** (1.986(4) Å) is the shortest thus far in a (cyclopentadienyl)ruthenium $\sigma$-acetylide complex, and one of the shortest thus far observed in a ruthenium $\sigma$-acetylide [6]. The C(1)–C(2) and C(2)–C(3) bonds (1.211(6) Å and 1.440(6) Å, respectively) are similar to those in other (cyclopentadienyl)ruthenium $\sigma$-acetylide complexes. Ru–C(1)–C(2) and C(1)–C(2)–C(3) angles (174.1(4) and 175.1(5)°, respectively) are close to linearity, with deviations probably due to packing effects. Bond and angle data for the phenyl rings in the acetylide ligand are consistent with the retention of aromaticity in the ground-state structure, with distances in the alkyne linkage consistent with a fully bond-alternated (C–C ≡ C–C) form rather than a cumulenyl (C=C=C=C) form. The phenyl rings are close to coplanarity (dihedral angle 18.80°), consistent with an extended $\pi$-system. Distances and angles within the phosphine and cyclopentadienyl ligands are not unusual.

### 2.3. Electrochemical studies

The electrochemical results obtained for complexes **7–10** are gathered in Table 3, together with previously reported data for related (cyclopentadienyl)ruthenium acetylides. We have previously noted that (i) ruthenium is oxidized at potentials approximately 0.2 V lower upon replacement of $PPh_3$ by $PMe_3$, i.e., upon increasing the donor strength of the phosphine, and that (ii) ruthenium is oxidized at potentials 0.2 V higher upon replacement of C ≡ CPh by 4-C ≡ $CC_6H_4NO_2$, i.e., upon increasing the acceptor strength of the acetylide. These data are consistent with a $Ru^{II/III}$ couple susceptible to variation in the electron-donating properties of the ligands [6]. The present work augments the earlier report by evaluating the effect of chain-lengthening upon electrochemical behaviour, for which a substantial decrease in oxidation potential at ruthenium (up to 0.2 V) is observed on proceeding from **6a** to **7–10**. More subtle variations (changing the bridging unit in the 'extended chain' acetylide complexes) do not affect the $Ru^{II}/Ru^{III}$ couple significantly, with oxidation potentials at 0.54 V (**7**), 0.55 V (**8**), 0.61 V (**9**) and 0.57 V (**10**). Trends in the electrochemical data thus mirror the $^{13}C$ NMR spectra (RuC, RuC ≡ *C* shifts), with appreciable changes in oxidation potential and chemical shifts upon ligand substitution ($PPh_3$ versus $PMe_3$), introduction of nitro-substituent (4-H versus 4-$NO_2$ phenylacetylide), and chain-lengthening (one-ring acetylide ligand versus two-ring acetylide ligand), but little variation in these data upon bridging unit modification across complexes **7–10**. Mulliken population analyses (Fig. 2) of complexes **7** and **9** employing ZINDO [23] are consistent with the spectral and electrochemical data, with differences in charge density localized at the varying bridging unit; charge density at both ruthenium and nitro group are similar for these two complexes. All $Ru^{II}/Ru^{III}$ oxidation waves for **7–10** are quasireversible; we have previously noted an increase in reversibility in proceeding from $PMe_3$ to $PPh_3$ [6]. Complexes **7–10** also contain reduction waves, assigned to reduction of the nitro substituent, which are signifi-

Table 3
Cyclic voltammetric data for (cyclopentadienyl)bis(phosphine)ruthenium complexes

| | $E^{\circ}_{Ru}$ (V) | $i_{pc}/i_{pa}$ | $E^{\circ}_{NO_2}$ (V) | $i_{pa}/i_{pc}$ |
|---|---|---|---|---|
| RuCl($PPh_3$)$_2$($\eta^5$-$C_5H_5$) (**3a**)[a,b] | 0.72 | 1.0 | | |
| RuCl($PMe_3$)$_2$($\eta^5$-$C_5H_5$) (**3b**)[a,b] | 0.42 | 1.0 | | |
| Ru(C ≡ CPh)($PPh_3$)$_2$($\eta^5$-$C_5H_5$) (**4a**)[a,c] | 0.55 | 0.7 | | |
| Ru(C ≡ CPh)($PPh_3$)$_2$($\eta^5$-$C_5H_5$) (**4a**)[d] | 0.54 | 0.5[e] | | |
| Ru(C ≡ CPh)($PMe_3$)$_2$($\eta^5$-$C_5H_5$) (**4b**)[a,c] | 0.37 | 0.2 | | |
| Ru(4-C ≡ $CC_6H_4NO_2$)($PPh_3$)$_2$($\eta^5$-$C_5H_5$) (**6a**)[a,c] | 0.73 | 1.0 | −1.08 | 1.0 |
| Ru(4-C ≡ $CC_6H_4NO_2$)($PMe_3$)$_2$($\eta^5$-$C_5H_5$) (**6b**)[a,c] | 0.52 | 0.3 | −1.10 | 1.0 |
| Ru(4,4′-C ≡ $CC_6H_4C_6H_4NO_2$)($PPh_3$)$_2$($\eta^5$-$C_5H_5$) (**7**)[a,b] | 0.54 | 0.8 | −0.96 | 0.9 |
| Ru((*E*)-4,4′-C ≡ $CC_6H_4CH{=}CHC_6H_4NO_2$)($PPh_3$)$_2$($\eta^5$-$C_5H_5$) (**8**)[a,b] | 0.55 | 0.9 | −0.92 | 0.3 |
| Ru(4,4′-C ≡ $CC_6H_4C$ ≡ $CC_6H_4NO_2$)($PPh_3$)$_2$($\eta^5$-$C_5H_5$) (**9**)[a,b] | 0.61 | 1.0 | −0.85 | 0.7 |
| Ru(4,4′-C ≡ $CC_6H_4N{=}CHC_6H_4NO_2$)($PPh_3$)$_2$($\eta^5$-$C_5H_5$) (**10**)[a,b] | 0.57 | 1.0 | −0.79 | 0.5 |
| Ru(C ≡ CPh)(dppe)($\eta^5$-$C_5H_5$)[d] | 0.48 | 0.5[e] | | |
| Ru(C ≡ CBu$^n$)($PPh_3$)$_2$($\eta^5$-$C_5H_5$)[d] | 0.48 | 0.7[f] | | |
| Ru(C ≡ CBu$^t$)($PPh_3$)$_2$($\eta^5$-$C_5H_5$)[d] | 0.47 | 0.9[f] | | |

[a] At −50°C vs. Ag/AgCl in $CH_2Cl_2$ with a rate of 100 mV $s^{-1}$ and a switching potential of 1.0 V. [b] 0.5 M [$NBu^n_4$][$PF_6$]. [c] Ref. [6]; 0.7 M [$NBu^n_4$][$PF_6$]. [d] Ref. [22]; room temperature, measured vs. SCE at a carbon electrode. Values quoted are referenced to Ag/AgCl electrode by applying a correction of 0.02 V. [e] Switching potential of 0.8 V. [f] Switching potential of 0.75 V.

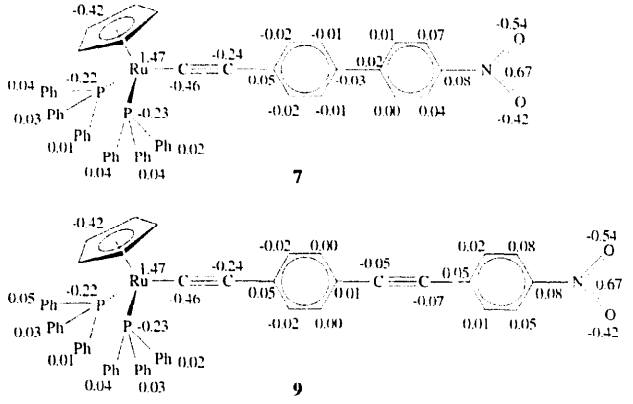

Fig. 2. Mulliken analyses for complexes **7** and **9**.

cantly less reversible than those of the one-ring acetylide complexes **6a,b**. Reduction potentials for **7–10** are more positive than those for **6a,b** and, as noted above, oxidation potentials are significantly less positive. The former are correlated with a nitro-centred LUMO and the latter with a metal-centred HOMO. Chain-lengthening leads then to a decrease in HOMO-LUMO separation manifested not only by an increase in UV-Vis $\lambda_{max}$, but also by a corresponding decrease in $(E^{o}_{Ru^{II}/Ru^{III}} - E^{o}_{NO_2/NO_2^-})$.

### 2.4. Quadratic hyperpolarizabilities

We have previously utilized ZINDO [23] to derive off-resonant quadratic nonlinearities for some (cyclopentadienyl)bis(phosphine)ruthenium $\sigma$-arylacetylides [6,7] and have now extended these studies to embrace the new acetylide complexes **7** and **9** and precursor chloride (Table 4). The optical nonlinearities for **3a,b** and **9** were calculated utilizing the crystallographically-derived coordinates, that for **7** being determined by using a combination of appropriate molecular fragments. The computed values are consistent with an increase in $\beta$ upon chain-lengthening; $\beta_{1907,calc}$ for **7** and **9** are both larger than $\beta_{1907,calc}$ for **6a**. These semi-empirical computation-derived data are consistent with a quadratic NLO efficiency sequence imino-linkage > *E*-ene-linkage > biphenyl linkage ≈ yne-linkage. Although Kanis et al. have shown that ZINDO can accurately reproduce experimental nonlinearities for a range of organometallic complexes [24], the validity of ZINDO as a predictor of NLO merit needs to be established for each complex type. We have therefore determined the nonlinearities of **7** and **9** experimentally by HRS; these data, together with the corresponding two-level corrected values, are given in Table 4.

The experimental data reveal an efficiency sequence *E*-ene-linkage > yne-linkage ≈ imino-linkage > biphenylene unit, but intense ($\varepsilon > 10000$) linear optical absorption maxima for all 'extended-chain' acetylide complexes within 100 nm of $2\omega$ are consistent with substantial dispersion enhancement of the observed nonlinearities. The quadratic nonlinearities for both **7** ($560 \times 10^{-30}$ cm$^5$ esu$^{-1}$) and **9** ($865 \times 10^{-30}$ cm$^5$ esu$^{-1}$) are very large for organometallic complexes. It has been suggested that the two-state model is appropriate in the limited cases where structural change is restricted to the molecular component responsible for the charge transfer band contributing to the hyperpolarizability [25]. It is likely that the higher energy bands are associated with transitions involving other ligands, with little change in dipole moment between ground and excited states, and hence only a small contribution to the optical nonlinearity projected onto the molecular dipole axis. The lack of contribution from transitions involving other ligands is also suggested by the low nonlinearity of the precursor chloride. Given the preceding, it is possible that the two-level corrected values may have some significance. The corrected nonlinearities suggest an efficiency series *E*-ene-linkage ≥ yne-linkage > biphenyl > imino-linkage, the first three paralleling relative merits in the 'all-organic' system [26]. Two-level adjusted values for both **7** ($134 \times 10^{-30}$ cm$^5$ esu$^{-1}$) and **9** ($212 \times 10^{-30}$ cm$^5$ esu$^{-1}$) are extremely large for organometallic com-

Table 4
Experimental[a] and ZINDO-derived linear optical spectroscopic and quadratic nonlinear optical response parameters

| | $\lambda$ (nm) ($\varepsilon$ ($10^4$ M$^{-1}$ cm$^{-1}$)) | $\beta^{b}_{1064}$ | $\beta^{c}_{1064,corr}$ | $\beta^{d}_{1907,calc}$ |
|---|---|---|---|---|
| RuCl(PPh$_3$)$_2$($\eta$-C$_5$H$_5$) (**3a**) | 357 (0.3) br, 290 (0.5) sh | < 7 | < 4 | 1 |
| RuCl(PMe$_3$)$_2$($\eta$-C$_5$H$_5$) (**3b**) | 347 (0.1) | e | e | 0 |
| Ru(C ≡ CPh)(PPh$_3$)$_2$($\eta$-C$_5$H$_5$) (**4a**) | 310 (2.0) | 16 | 10 | 2 |
| Ru(C ≡ CPh)(PMe$_3$)$_2$($\eta$-C$_5$H$_5$) (**4b**) | 320 (1.6) | e | e | 5 |
| Ru(4-C ≡ CC$_6$H$_4$NO$_2$)(PPh$_3$)$_2$($\eta$-C$_5$H$_5$) (**6a**) | 460 (1.1), 382 (1.1) | 468 | 96 | 29 |
| Ru(4-C ≡ CC$_6$H$_4$NO$_2$)(PMe$_3$)$_2$($\eta$-C$_5$H$_5$) (**6b**) | 477 (1.7), 279 (1.0) | 248 | 38 | 31 |
| Ru(4,4'-C ≡ CC$_6$H$_4$C$_6$H$_4$NO$_2$)(PPh$_3$)$_2$($\eta$-C$_5$H$_5$) (**7**) | 448 (1.6), 310 (2.3) | 560 | 134 | 36 |
| Ru((*E*)-4,4'-C ≡ CC$_6$H$_4$CH=CHC$_6$H$_4$NO$_2$)(PPh$_3$)$_2$($\eta$-C$_5$H$_5$) (**8**) | 476 (2.6), 341 (2.4) | 1455 | 232 | 45 |
| Ru(4,4'-C ≡ CC$_6$H$_4$C ≡ CC$_6$H$_4$NO$_2$)(PPh$_3$)$_2$($\eta$-C$_5$H$_5$) (**9**) | 446 (1.9), 340 (2.8) | 865 | 212 | 36 |
| Ru(4,4'-C ≡ CC$_6$H$_4$N=CHC$_6$H$_4$NO$_2$)(PPh$_3$)$_2$($\eta$-C$_5$H$_5$) (**10**) | 496 (1.3), 298 (2.6) | 840 | 86 | 55 |

[a] All measurements in thf solvent. All complexes are optically transparent at 1064 nm. [b] HRS at 1064 nm; values ±10%. [c] HRS at 1064 nm corrected for resonance enhancement at 532 nm using the two-level model with $\beta_0 = \beta[1 - (2\lambda_{max}/1064)^2][1 - (\lambda_{max}/1064)^2]$; damping factors not included. [d] ZINDO derived data at 1907 nm. [e] Not measured.

Table 5
Experimental linear optical spectroscopic and cubic nonlinear optical response parameters[a]

| | λ (nm) (ε ($10^4$ $M^{-1}$ $cm^{-1}$)) | γ($10^{-36}$ esu)[b] | | |
|---|---|---|---|---|
| | | DFWM (real part) | Z-scan (real part) | Z-scan (imag. part) |
| $RuCl(PPh_3)_2(\eta\text{-}C_5H_5)$ **(3a)** | 357 (0.3) br, 290 (0.5) sh | 50 ± 20 | 150 ± 100 | |
| $RuCl(PMe_3)_2(\eta\text{-}C_5H_5)$ **(3b)** | 347 (0.1) | 80 ± 30 | ≤ 80 | |
| $Ru(C\equiv CPh)(PPh_3)_2(\eta\text{-}C_5H_5)$ **(4a)** | 310 (2.0) | | ≤ 150 | |
| $Ru(4\text{-}C\equiv CC_6H_{4[35]}Br)(PPh_3)_2(\eta\text{-}C_5H_5)$ **(5)** | 325 (3.2) | | ≤ 150 | |
| $Ru(4\text{-}C\equiv CC_6H_4NO_2)(PPh_3)_2(\eta\text{-}C_5H_5)$ **(6a)** | 460 (1.1), 382 (1.1) | −260 ± 60 | −210 ± 50 | ≤ 10 |
| $Ru(4\text{-}C\equiv CC_6H_4NO_2)(PMe_3)_2(\eta\text{-}C_5H_5)$ **(6b)** | 477 (1.7), 279 (1.0) | | −230 ± 70 | 74 ± 30 |
| $Ru(4,4'\text{-}C\equiv CC_6H_4C_6H_4NO_2)(PPh_3)_2(\eta\text{-}C_5H_5)$ **(7)** | 448 (1.6), 310 (2.3) | | −380 ± 200 | 320 ± 160 |
| $Ru((E)\text{-}4,4'\text{-}C\equiv CC_6H_4CH{=}CHC_6H_4NO_2)(PPh_3)_2(\eta\text{-}C_5H_5)$ **(8)** | 476 (2.6), 341 (2.4) | | −450 ± 100 | 210 ± 60 |
| $Ru(4,4'\text{-}C\equiv CC_6H_4C\equiv CC_6H_4NO_2)(PPh_3)_2(\eta\text{-}C_5H_5)$ **(9)** | 446 (1.9), 340 (2.8) | | −450 ± 100 | ≤ 20 |
| $Ru(4,4'\text{-}C\equiv CC_6H_4N{=}CHC_6H_4NO_2)(PPh_3)_2(\eta\text{-}C_5H_5)$ **(10)** | 496 (1.3), 298 (2.6) | | −850 ± 300 | 360 ± 200 |

[a] All measurements as thf solutions (all complexes are optically transparent at 800 nm). [b] All results are referenced to the hyperpolarizability of thf $\gamma = 1.6 \times 10^{-36}$ esu.

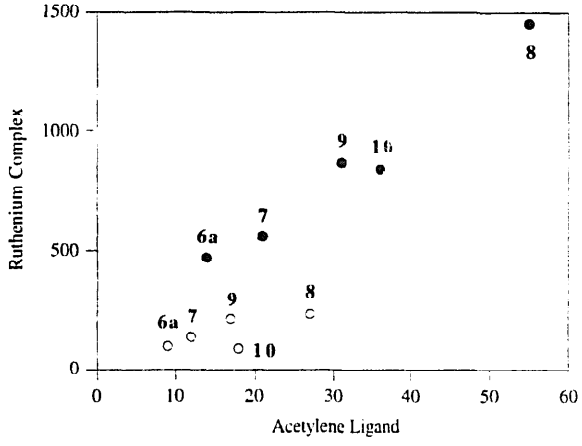


Fig. 3. Correlation of molecular quadratic hyperpolarizabilities of complexes **6a**, **7–10** with those of the corresponding terminal alkynes ($10^{-30}$ cm$^5$ esu$^{-1}$); (●) experimental; (○) two-level corrected.

plexes, the latter in particular suggesting that yne-linkage may be worthy of consideration for the preparation of longer chromophores (while the nonlinearities of **8** and **9** are comparable, complex **9** involves less trade-off in optical transparency).

We have previously correlated quadratic nonlinearities of (triphenylphosphine)gold acetylide complexes with precursor acetylenes [12]. Excluding data for Au((*Z*)-4,4′-C ≡ $CC_6H_4CH{=}CHC_6H_4NO_2$)($PPh_3$) (which fluoresced significantly), a linear correlation for both uncorrected and two-level-corrected data was observed, with the slopes of the graphs (2.4 ($R = 0.99$) for uncorrected; 2.0 ($R = 0.99$) for two-level-corrected) defining a 'figure of merit' for the (triphenylphosphine)gold unit compared to hydrogen. We have extended this comparison to the (cyclopentadienyl)bis(triphenylphosphine)ruthenium system, the data for which are displayed in Fig. 3. The 'figures of merit' for the ligated ruthenium are larger than for the ligated gold, although the correlation coefficients are not as good (24 ($R = 0.98$) for uncorrected; 6.7 ($R = 0.69$) for two-level corrected). The poor correlation stems from the smaller-than-expected two-level-corrected nonlinearities for **8** and (particularly) **10**, the complexes with $\lambda_{max}$ closest to $2\omega$, perhaps suggesting that for **8** and **10** the two-level correction is inappropriate. The two level correction neglects damping, an approximation which becomes less tenable the closer $\lambda_{max}$ is to $2\omega$. It is therefore almost certain that $\beta_{corr}$ for **10** is a serious underestimation, and $\beta_{corr}$ for **8** may be reduced somewhat also. The evidence is compelling, though, that the $Ru(PPh_3)_2(\eta\text{-}C_5H_5)$ moiety is a much more efficient donor than $Au(PPh_3)$ for enhancing quadratic optical nonlinearity, perhaps understandable as the 18 electron ruthenium in the former is more electron rich than the 14 electron gold in the latter.

### 2.5. Cubic hyperpolarizabilities

Third-order nonlinearities were evaluated by Z-scan with some additional experiments performed using DFWM; the latter provides information about the temporal behaviour of the nonlinearity, in the present case confirming the electronic origin of the observed response. Cubic optical nonlinearities by both techniques are given in Table 5.

As with the quadratic optical nonlinearities above, the observed cubic responses are not simply the sums of nonlinearities for the molecular fragments; $\gamma$ for **6b** is much larger than that of **3b** and 4-ethynylnitrobenzene ($20 \times 10^{-36}$ esu), indicating that electronic communication between the ligated metal and acetylide fragments is important. Only one pair of complexes varying in their phosphine (**6a,b**) give sufficiently large nonlinearities to permit comparison. Proceeding from **6a** to **6b** makes little difference to $\gamma$, although a 50% decrease in response was noted with the corresponding $\beta$ values. We have recently observed differing effects on $\beta$ and $\gamma$ values in proceeding from Au(4,4′-C ≡ $CC_6H_4C \equiv CC_6H_4NO_2$)($PPh_3$) to Au((*E*)-4,4′-C ≡ $CC_6H_4CH{=}CHC_6H_4NO_2$)($PPh_3$) ($\beta$ increases sharply, $\gamma$ decreases marginally) [27,12]. Thus, results from both the gold and ruthenium systems suggest that structural modifications which enhance $\beta$ do not necessarily increase $\gamma$. Whereas minor variation in the acetylide ligand (replacement of 4-H by 4-Br in proceeding from (**4a**) to (**5**)) has no effect on $\gamma$, introduction of the strongly-withdrawing $NO_2$ (in proceeding to (**6a**)) makes a significant difference and also results in a reversal of sign.

In our preliminary report [8], we discussed the origin of the negative nonlinearities observed with the nitro-containing complexes. Thermal lensing and bond-length-alternation effects were eliminated as the origin of negative $\gamma$, and two-photon dispersion was deemed likely, but a negative static hyperpolarizability could not be ruled out. All complexes with negative $\gamma$ have $\lambda_{max}$ longer than 400 nm, and all complexes with positive $\gamma$ have $\lambda_{max}$ shorter than 400 nm. We have now determined cubic optical nonlinearities for **7** and **9**, and once again $\lambda_{max}$ longer than 400 nm is associated with negative nonlinearities. Recently, we have coupled these nitro-containing alkynyl ligands to (triphenylphosphine)gold(I), resulting in a series of complexes with $\lambda_{max}$ shorter than 400 nm and uniformly positive nonlinearities [27]. While these data are not conclusive, they strongly support the contention that the dispersion effect of two-photon states is contributing to the observed responses, rather than the complexes possessing frequency-independent negative nonlinearities.

Not surprisingly, extension from a one-ring chromophore (**6a**) to extended chain two-ring chromophores

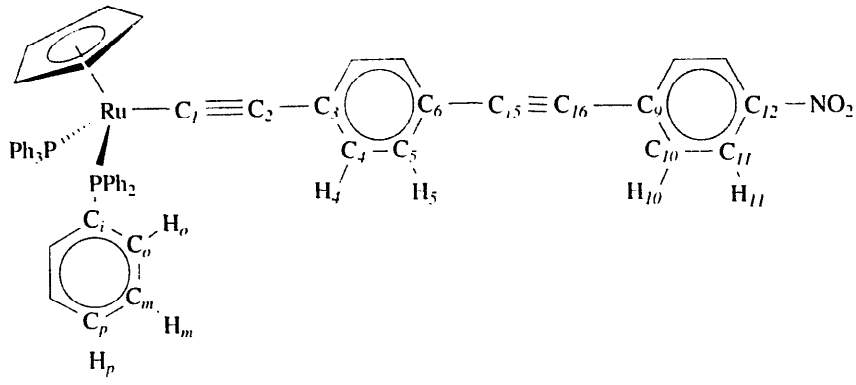

Fig. 4. Numbering scheme for NMR spectral assignment of **9**. Analogous scheme for **1**, **2** and **7**.

**(7–10)** leads to a large increase in $\gamma$, which parallels results from the 'all-organic' system. Errors associated with the real components of $\gamma$ for **7–10**, and the significant imaginary components of the nonlinearities of these complexes, render comparison of the effect of bridging unit variation upon $\gamma$ meaningless: measurements at longer wavelengths are required to resolve this.

## 3. Conclusion

The systematically-varied series of organometallic donor-bridge-acceptor acetylide complexes permit a number of comments to be made. X-ray structural studies of most of the complexes have been carried out, with little variation in RuC and C ≡ C parameters, and no evidence for a substantial vinylidene contributor to the ground state geometry. $^{13}C$ NMR spectral data (RuC, RuC ≡ *C* chemical shifts) and electrochemical data ($Ru^{II/III}$ potentials) are sensitive to phosphine replacement, introduction of alkynyl nitro substituent, and alkynyl chain-lengthening, but insensitive to two-ring acetylide bridge modification. Charge density calculations and spectral data are consistent with two-ring acetylide bridge modification inducing electron density variations at the bridging unit only. Computationally-derived (ZINDO), dispersion enhanced experimentally obtained (HRS) and two-level corrected quadratic nonlinearities increase on chain-lengthening from one-ring to biphenyl and yne-linked two-ring acetylide ligand, with the ene-linked two-ring acetylide the most efficient, and absolute values for the ene-linked and yne-linked very large for organometallic complexes. Cubic nonlinearities are electronic in origin. Nitro-containing complexes have negative $\gamma$ at 800 nm, probably due to two-photon dispersion. Chain-lengthening leads to an increase in molecular third-order hyperpolarizability, but relative $\gamma$ values do not mirror relative $\beta$ values for this series of complexes. The (cyclopentadienyl)bis(triphenylphosphine)ruthenium complexes have larger $\beta$ values than their (triphenylphosphine)gold analogues, with the efficiency of the ligated metal as a donor group related to its metal valence electron count. In contrast, some of the $\gamma$ values for gold complexes are larger than those of their ruthenium analogues, emphasizing that enhancing cubic optical nonlinearities of organometallic complexes does not simply involve increasing quadratic NLO merit. Further studies with systematically varied complexes are currently underway.

## 4. Experimental

### 4.1. General

All organometallic reactions were carried out under an atmosphere of nitrogen with the use of standard Schlenk techniques; no attempt was made to exclude air during work-up of organometallic products or while carrying out syntheses of organic compounds. Petroleum ether refers to a fraction of boiling range 60–80°C. Commercial reagents trimethylsilylacetylene, copper(I) iodide, 4-diiodobenzene, 4-iodonitrobenzene and 4-nitrobiphenyl (Aldrich) were used as received. 4-Diethynylbenzene [16], 4,4′-bromonitrobiphenyl [15], $PdCl_2(PPh_3)_2$ [28], $RuCl(PPh_3)_2(\eta\text{-}C_5H_5)$ **(3a)** [29], $RuCl(Ph_3)_2(\eta\text{-}C_5H_5)$ **(3b)** [30], $Ru(C \equiv CPh)(PPh_3)_2(\eta\text{-}C_5H_5)$ **(4a)** [17], $Ru(C \equiv CPh)(PMe_3)_2(\eta\text{-}C_5H_5)$ **(4b)** [31], $Ru(4\text{-}C \equiv CC_6H_4Br)(P_3)_2(\eta\text{-}C_5H_5)$ **(5)** [32], $Ru(4\text{-}C \equiv CC_6H_4NO_2)(PPh_3)_2(\eta\text{-}C_5H_5)$ **(6a)** [6], $Ru(4\text{-}C \equiv CC_6H_4NO_2)(PMe_3)_2(\eta\text{-}C_5H_5)$ **(6b)** [6], Ru((*E*)-4,4′-C ≡ $CC_6H_4CH{=}CHC_6H_4NO_2$)$(PPh_3)_2(\eta\text{-}C_5H_5)$ **(8)** [7], and $Ru(4,4'\text{-}C \equiv CC_6H_4N{=}CHC_6H_4\text{-}NO_2)(PPh_3)_2(\eta\text{-}C_5H_5)$ **(10)** [7], were prepared following the literature methods. Thin layer chromatography was carried out using 7749 Kieselgel 60 $PF_{254}$ silica (Merck). Column chromatography was carried out using 7734 Kieselgel 60 silica (Merck). Microanalyses were performed at the Research School of Chemistry, Australian National University. Infrared spectra were recorded using a Perkin–Elmer 1600 or System 2000 FT-IR spectrometer. UV-Visible spectra were recorded

using a Cary 5 spectrophotometer. Electrochemical measurements were carried out using a Princeton Applied Research Model 170 Potentiostat. The supporting electrolyte was $[NBu^n_4][PF_6]$ in distilled deoxygenated $CH_2Cl_2$. Solutions ($1 \times 10^{-3}$ M) were made under a purge of nitrogen and measured versus a Ag/AgCl reference electrode at −50°C, such that the ferrocene/ferrocenium redox couple was located at 0.55 V.

$^1H$, $^{13}C$ and $^{31}P$ NMR spectra were recorded using a Varian Gemini-300 FT NMR spectrometer and are referenced to residual $CHCl_3$, 7.24 ppm, $CDCl_3$, 77.0 ppm, and external 85% $H_3PO_4$, 0.0 ppm, respectively. NMR spectral assignments for **9** follow the numbering scheme shown in Fig. 4. Compounds **1**, **2** and **7** are numbered analogously.

### 4.2. Syntheses of terminal alkynes and acetylide complexes

#### 4.2.1. 4,4'-HC≡CC$_6$H$_4$C$_6$H$_4$NO$_2$ (1)

4,4'-Bromonitrobiphenyl (2.0 g, 7.2 mmol), trimethylsilylacetylene (1.4 ml, 9.9 mmol), $PdCl_2(PPh_3)_2$ (50 mg, 0.071 mmol) and CuI (5 mg, 0.03 mmol) were added to triethylamine (20 ml). The mixture was heated at 80°C for 12 h in a closed tube, cooled, filtered, and the solvent removed from the filtrate under reduced pressure. The residue was dissolved in methanol (50 ml). Sodium hydroxide (50 ml of a 1 M solution in water) was added and the mixture stirred for 6 h. The methanol was removed under reduced pressure and the suspension extracted with dichloromethane. The resultant dichloromethane solution was dried over anhydrous magnesium sulfate, filtered, and the filtrate reduced to dryness and purified by column chromatography (1:4 $CH_2Cl_2$:petroleum ether) yielding 0.96 g (60%) of **1** as a pale yellow solid. Anal. Calcd. for $C_{14}H_9NO_2$: C 75.33, H 4.06, N 6.27%. Found: C 75.11, H 4.31, N 6.07%. $^1H$ NMR: (δ, 300 MHz, $CDCl_3$): 3.18 (s, 1H, $H_1$), 7.57, 7.60 (2d, $J_{HH}$ = 8 Hz, 4H, $H_4$, $H_5$), 7.72 (d, $J_{HH}$ = 9 Hz, 2H, $H_{10}$), 8.29 (d, $J_{HH}$ = 9 Hz, 2H, $H_{11}$). $^{13}C$ NMR: (δ, 75 MHz, $CDCl_3$); 78.9 ($C_1$), 82.9 ($C_2$), 122.8 ($C_3$), 124.2 ($C_{11}$), 127.3, 127.7 ($C_5$, $C_{10}$), 132.8 ($C_4$), 138.9 ($C_6$), 146.5 ($C_9$), 147.3 ($C_{12}$).

#### 4.2.2. 4,4'-HC≡CC$_6$H$_4$C≡CC$_6$H$_4$NO$_2$ (2)

4-Diethynylbenzene (300 mg, 2.4 mmol), 4-iodonitrobenzene (200 mg, 0.80 mmol), $PdCl_2(PPh_3)_2$ (10 mg, 0.014 mmol) and CuI (5 mg, 0.03 mmol) were stirred in diethylamine (50 ml) at room temperature for 4 h. The diethylamine was removed under reduced pressure, water added (100 ml), and the residue extracted with diethylether. The ethereal phase was separated and dried over anhydrous magnesium sulfate, filtered, and reduced to dryness. The residue was washed through a silica plug with petroleum ether (300 ml) to remove excess diethynylbenzene, and $CH_2Cl_2$ to remove the product which was purified by thin layer chromatography, yielding 130 mg (66%) of **2** as a yellow solid. Anal. Calcd. for $C_{16}H_9NO_2$: C 77.72, H 3.68, N 5.67%. Found: C 77.96, H 4.13, N 5.37%. $^1H$ NMR: (δ, 300 MHz, $CDCl_3$); 3.19 (s, 1H, $H_1$), 7.49 (s, 4H, $H_4$, $H_5$), 7.65 (d, $J_{HH}$ = 9 Hz, 2H, $H_{10}$), 8.21 (d, $J_{HH}$ = 9 Hz, 2H, $H_{11}$). $^{13}C$ NMR: (δ, 75 MHz, $CDCl_3$); 79.6 ($C_1$), 83.0 ($C_2$), 89.3 ($C_{15}$), 93.9 ($C_{16}$), 122.4, 122.9 ($C_3$, $C_6$), 123.6 ($C_{11}$), 129.8 ($C_9$), 131.7, 132.2, 132.3 ($C_4$, $C_5$, $C_{10}$), 147.1 ($C_{12}$).

#### 4.2.3. Ru(4,4'-C≡CC$_6$H$_4$C$_6$H$_4$NO$_2$)(PPh$_3$)$_2$(η-C$_5$H$_5$) (7)

$RuCl(PPh_3)_2(\eta\text{-}C_5H_5)$ (200 mg, 0.28 mmol) and 4,4'-HC≡CC$_6$H$_4$C$_6$H$_4$NO$_2$ (70 mg, 0.31 mmol) were refluxed in MeOH (10 ml) for 30 min and the solution allowed to cool to room temperature. A solution of sodium methoxide in methanol (6 ml, 0.1 M) was added and the solvent volume then reduced to 5 ml. Filtration afforded the product **7** as a red powder (105 mg, 42%). Anal. Calcd. for $C_{55}H_{43}NO_2P_2Ru$: C 72.35, H 4.76, N 1.53%. Found: C 72.20, H 4.64, N 1.26%. IR: (cyclohexane) ν(C≡C) 2074 cm$^{-1}$; ($CH_2Cl_2$) ν(C≡C) 2068 cm$^{-1}$. $^1H$ NMR: (δ, 300 MHz, $CDCl_3$); 4.33 (s, 5H, $C_5H_5$), 7.08 (t, $J_{HH}$ = 7 Hz, 12H, $H_m$), 7.18 (d, $J_{HH}$ = 8 Hz, 2H, $H_4$), 7.19 (m, 6H, $H_p$), 7.44 (d, $J_{HH}$ = 8 Hz, 2H, $H_5$), 7.45 (m, 12H, $H_o$), 7.70 (d, $J_{HH}$ = 9 Hz, 2H, $H_{10}$), 8.24 (d, $J_{HH}$ = 9 Hz, 2H, $H_{11}$). $^{13}C$ NMR: (δ, 75 MHz, $CDCl_3$); 85.3 ($C_5H_5$), 114.9 ($C_3$), 124.1 ($C_{11}$), 124.2 (t, $J_{CP}$ = 25 Hz, $C_i$), 126.7, 126.8 ($C_5$, $C_{10}$), 127.2 (t, $J_{CP}$ = 5 Hz, $C_m$), 128.5 ($C_p$), 131.1 ($C_4$), 131.6 ($C_3$), 132.4 ($C_6$), 133.6 (t, $J_{CP}$ = 5 Hz, $C_o$), 138.7 (m, $C_i$), 146.1 ($C_{12}$), 147.8 ($C_9$). $^{31}P$ NMR: (δ, 121 MHz, $CDCl_3$); 51.2.

#### 4.2.4. Ru(4,4'-C≡CC$_6$H$_4$C≡CC$_6$H$_4$NO$_2$)(PPh$_3$)$_2$(η-C$_5$H$_5$) (9)

Following the method for **7**, $RuCl(PPh_3)_2(\eta\text{-}C_5H_5)$ (50 mg, 0.07 mmol), 4,4'-HC≡CC$_6$H$_4$C≡CC$_6$H$_4$NO$_2$ (**2**) (20 mg, 0.08 mmol) and sodium methoxide in methanol (3 ml, 0.1 M) afforded **9** as a red microcrystalline solid (57 mg, 88%). Anal. Calcd. for $C_{57}H_{43}NO_2P_2Ru$: C 73.07, H 4.63, N 1.50%. Found: C 72.82, H 4.47, N 1.19%. IR: (cyclohexane) ν(C≡C) 2070 cm$^{-1}$; ($CH_2Cl_2$) ν(C≡C) 2065 cm$^{-1}$. $^1H$ NMR: (δ, 300 MHz, $CDCl_3$); 4.32 (s, 5H, $C_5H_5$), 7.03 (d, $J_{HH}$ = 8 Hz, 2H, $H_4$), 7.07 (t, $J_{HH}$ = 7 Hz, 12H, $H_m$), 7.19 (t, $J_{HH}$ = 7 Hz, 6H, $H_p$), 7.32 (d, $J_{HH}$ = 8 Hz, 2H, $H_5$), 7.44 (m, 12H, $H_o$), 7.60 (d, $J_{HH}$ = 9 Hz, 2H, $H_{10}$), 8.18 (d, $J_{HH}$ = 9 Hz, 2H, $H_{11}$). $^{13}C$ NMR: (δ, 75 MHz, $CDCl_3$); 85.3 ($C_5H_5$), 87.0 ($C_{15}$), 96.8 ($C_{16}$), 115.5, 115.7 ($C_2$, $C_6$), 123.6 ($C_{11}$), 126.6 (t, $J_{CP}$ = 25 Hz, $C_i$), 127.3 (t, $J_{CP}$ = 5 Hz, $C_m$), 128.5 ($C_p$), 130.5, 131.4, 131.8 ($C_4$, $C_5$, $C_{10}$), 131.0 ($C_9$), 133.7 (t, $J_{CP}$ = 5 Hz, $C_o$), 138.6 (m, $C_i$), 146.4 ($C_{12}$), ($C_3$ obscured). $^{31}P$

NMR: ($\delta$, 121 MHz, $CDCl_3$); 51.0. A crystal suitable for X-ray diffraction analysis was grown from slow diffusion of hexane into a dichloromethane solution.

### 4.3. X-ray crystallography

Measurements were made using a Rigaku AFC6S diffractometer, with graphite monochromated Mo–K$\alpha$ (0.7107 Å) radiation, on a red crystal of approximate dimensions $0.2 \times 0.2 \times 0.2$ mm$^3$ mounted on a glass fibre. Cell constants obtained from 25 carefully centred reflections ($34 < 2\theta < 42°$) corresponded to a primitive monoclinic cell, space group $P2_1/n$ (No. 14), with dimensions: $a = 10.842(1)$, $b = 19.792(4)$, $c = 21.200(2)$ Å and $\beta = 100.81(2)°$ ($V = 4468(1)$ Å$^3$). For $Z = 4$ and $FW = 937.0$, $D_{calc} = 1.39$ g cm$^{-3}$. The data were collected at 23°C using the $\omega$–$2\theta$ scan mode (scan rate = 2.0° min$^{-1}$ (in $\omega$); take off angle = 6°; $2\theta_{max} = 50.1°$). Of the 8153 independent reflections, 5416 were considered observed ($I > 3.0\sigma(I)$). An empirical absorption correction was applied ($\mu = 4.6$ cm$^{-1}$, $T_{min} = 0.83$, $T_{max} = 1.00$). The data were corrected for Lorentz and polarization effects. No decay correction was required. The structure was solved by Patterson heavy-atom methods and expanded using Fourier techniques. The non-hydrogen atoms were refined anisotropically. Hydrogen atoms were included at calculated positions but not refined. The final cycle of least-squares refinement converged with weighted and unweighed agreement factors of $R = \Sigma||F_o| - |F_c||/\Sigma|F_o| = 0.039$ and $R_w = [\Sigma w(|F_o| - |F_c|)^2/\Sigma wF_o^2]^{1/2} = 0.037$ where $w = 4F_o^2/\sigma^2(F_o)$; $\sigma^2(F_o) = [S^2(C + 4B) + (pF_o^2)^2]/L_p^2$ ($S$ = scan rate, $C$ = peak count, $B$ = background count, $L_p$ = Lorentz polarization factor, $p = 0.008$ determined experimentally from standard reflections). The maximum and minimum peaks in the final difference Fourier map corresponded to 0.69 and −0.55 e Å$^{-3}$ respectively. Neutral atom scattering factors were used. All calculations were performed using the teXsan crystallographic software package [33].

### 4.4. Computational details

Results were obtained using ZINDO [23] (June 1994 version) from Biosym Technologies, San Diego, implemented on a Silicon Graphics INDY workstation without parameter manipulation or basis function alteration. Calculations for **3a,b** and **9** used crystallographically-derived atomic coordinates as input data. For **7**, coordinates were produced from a combination of fragments of related structurally characterized complexes $(Ru(PPh_3)_2(\eta\text{-}C_5H_5)$ from **9**, and 4,4′-C ≡ $CC_6H_4C_6H_4NO_2$ from $Au(4,4'\text{-}C \equiv CC_6H_4C_6H_4NO_2)(PPh_3)$ [12]. An Ru–C distance of 1.99 Å was assumed). CI calculations included single excitations; basis set sizes were increased progressively for all calculations until convergence ($\pm 2 \times 10^{30}$ cm$^5$ esu$^{-1}$) in the computed $\beta_{vec}$ value was reached (260–300 excited configurations).

### 4.5. HRS measurements

An injection-seeded Nd:YAG laser (Q-switched Nd:YAG Quanta Ray GCR5, 1064 nm, 8 ns pulses, 10 Hz) was focused into a cylindrical cell (7 ml) containing the sample. The intensity of the incident beam was varied by rotation of a half-wave plate placed between crossed polarizers. Part of the laser pulse was sampled by a photodiode to measure the vertically polarized incident light intensity. The frequency doubled light was collected by an efficient condenser system and detected by a photomultiplier. The harmonic scattering and linear scattering were distinguished by appropriate filters; gated integrators were used to obtain intensities of the incident and harmonic scattered light. All measurements were performed in thf using $p$-nitroaniline ($\beta = 21.4 \times 10^{-30}$ cm$^5$ esu$^{-1}$) [34] as a reference. Further details of the experimental procedure have been reported elsewhere [35–37].

### 4.6. Z-scan measurements

Measurements were performed at 800 nm using a system consisting of a Coherent Mira Ar-pumped Ti-sapphire laser generating a mode-locked train of approximately 100 fs pulses and a home-built Ti-sapphire regenerative amplifier pumped with a frequency-doubled Q-switched pulsed YAG laser (Spectra Physics GCR) at 30 Hz and employing chirped pulse amplification. Thf solutions were examined in a glass cell with a 0.1 cm path length. The Z-scans were recorded at two concentrations for each compound and the real and imaginary part of the nonlinear phase change determined by numerical fitting [38]. The real and imaginary part of the hyperpolarizability of the solute was then calculated by assuming linear concentration dependencies of the nonlinearities. The nonlinearities and light intensities were calibrated using measurements of a 1 mm thick silica plate for which the nonlinear refractive index $n_2 = 3 \times 10^{-16}$ cm$^2$ W$^{-1}$ was assumed.

### 4.7. DFWM measurements

DFWM measurements were performed with 100 fs 800 nm laser pulses derived from the same laser system as Z-scan. Forward (BOXCARS) geometry of the DFWM setup was used. Time-dependent DFWM signals were recorded for the samples investigated (solutions of the compounds in 1 mm glass cells) by optically delaying one of the three beams incident on the sample. The intensities of the DFWM signals were then

used for the calculation of the sample nonlinearity. The relation between the DFWM signal and the third-order nonlinear susceptibility $\chi^{(3)}$ was taken as $I_{DFWM} \propto |\chi^{(3)}|^2 L^2$, where $L$ is the sample thickness. The nonlinear susceptibility of solutions was assumed to be $\chi^{(3)} = L^4 \Sigma_i N_i \gamma_i$, where $L = (n^2 + 2)/3$ is the Lorenz local field factor ($n$ being the refractive index), $N_i$ is the concentration of molecules of a given kind and $\gamma_i$ is their hyperpolarizability.

## Acknowledgements

We thank the Australian Research Council (MGH), Telstra (MGH), the Belgian Government (Grant No. IUAP-P4/11) (AP), the Fund for Scientific Research-Flanders (Grant Nos. G.0308.96) (AP), the University of Leuven (Grant No. GOA 95/1) (AP) for support of this work, and Johnson–Matthey Technology Centre (MGH) for the loan of ruthenium salts. Dr. D. Ollis is thanked for access to an INDY workstation and Mr. D. Bogsányi for obtaining UV-Visible spectra. I.R.W. is the recipient of an Australian Postgraduate Research Award (Industry), M.P.C. holds an ARC Australian Postdoctoral Research Fellowship, M.G.H. holds an ARC Australian Research Fellowship, and S.H. is a Research Assistant of the Fund for Scientific Research-Flanders.

## References

[1] N.J. Long, Angew. Chem., Int. Ed. Engl. 34 (1995) 21.
[2] S.R. Marder, in: D.W. Bruce, D. O'Hare (Eds.), Inorganic Materials, Wiley, Chichester, England, 1992, p. 115.
[3] H.S. Nalwa, Appl. Organomet. Chem. 5 (1991) 349.
[4] I.R. Whittall, A.M. McDonagh, M.G. Humphrey, M. Samoc, Adv. Organomet. Chem., in press.
[5] I.R. Whittall, A.M. McDonagh, M.G. Humphrey, M. Samoc, Adv. Organomet. Chem., in press.
[6] I.R. Whittall, M.G. Humphrey, D.C.R. Hockless, B.W. Skelton, A.H. White, Organometallics 14 (1995) 3970.
[7] I.R. Whittall, M.G. Humphrey, A. Persoons, S. Houbrechts, Organometallics 15 (1996) 1935.
[8] I.R. Whittall, M.G. Humphrey, M. Samoc, J. Swiatkiewicz, B. Luther-Davies, Organometallics 14 (1995) 5493.
[9] A.M. McDonagh, I.R. Whittall, M.G. Humphrey, B.W. Skelton, A.H. White, J. Organomet. Chem. 519 (1996) 229.
[10] A.M. McDonagh, I.R. Whittall, M.G. Humphrey, D.C.R. Hockless, B.W. Skelton, A.H. White, J. Organomet. Chem. 523 (1996) 33.
[11] A.M. McDonagh, M.P. Cifuentes, I.R. Whittall, M.G. Humphrey, M. Samoc, B. Luther-Davies, D.C.R. Hockless, J. Organomet. Chem. 526 (1996) 99.
[12] I.R. Whittall, M.G. Humphrey, S. Houbrechts, A. Persoons, D.C.R. Hockless, Organometallics 15 (1996) 5738.
[13] S. Houbrechts, K. Clays, A. Persoons, V. Cadierno, M.P. Gamasa, J. Gimeno, I.R. Whittall, M.G. Humphrey, Proc. SPIE-Int Soc. Opt. Eng. 2852 (1996) 98.
[14] M.G. Humphrey, Chem. Aust. 63 (1996) 442.
[15] R.J.W. Le Fèvre, E.E. Turner, J. Chem. Soc. (1926) 2041.
[16] S. Takahashi, Y. Kuroyama, K. Sonogashira, N. Hagihara, Synthesis, (1980) 627.
[17] M.I. Bruce, R.C. Wallis, Aust. J. Chem. 32 (1979) 1471.
[18] M. Sato, H. Shintate, Y. Kawata, M. Sekino, Organometallics 13 (1994) 1956.
[19] M.I. Bruce, M.G. Humphrey, M.R. Snow, E.R.T. Tiekink, J. Organomet. Chem. 314 (1986) 213.
[20] J.M. Wisner, T.J. Bartczak, J.A. Ibers, Inorg. Chim. Acta 100 (1985) 115.
[21] G. Consiglio, F. Morandini, A. Sironi, J. Organomet. Chem. 306 (1986) C45.
[22] C. Bitcon, M.W. Whiteley, J. Organomet. Chem. 336 (1987) 385.
[23] ZINDO User Guide, Biosym Technologies, San Diego, 1994.
[24] D.R. Kanis, M.A. Ratner, T.J. Marks, J. Am. Chem. Soc. 114 (1992) 10338.
[25] L.-T. Cheng, W. Tam, S.H. Stevenson, G.R. Meredith, G. Rikken, S.R. Marder, J. Phys. Chem. 95 (1991) 10631.
[26] L.-T. Cheng, W. Tam, S.R. Marder, A.E. Stiegman, G. Rikken, C.W. Spangler, J. Phys. Chem. 95 (1991) 10643.
[27] I.R. Whittall, M.G. Humphrey, M. Samoc, B. Luther-Davies, Angew. Chem., Int. Ed. Engl. 36 (1997) 370.
[28] R.F. Heck, Palladium Reagents in Organic Syntheses, Academic Press, London, England, 1985.
[29] M.I. Bruce, C. Hameister, A.G. Swincer, R.C. Wallis, Inorg. Synth. 21 (1982) 78.
[30] M.I. Bruce, F.-S. Wong, B.W. Skelton, A.H. White, J. Chem. Soc., Dalton Trans. (1981) 1398.
[31] M.I. Bruce, F.-S. Wong, B.W. Skelton, A.H. White, J. Chem. Soc., Dalton Trans. (1982) 2203.
[32] M.I. Bruce, G.A. Koutsantonis, M.J. Liddell, B.K. Nicholson, J. Organomet. Chem. 320 (1987) 217.
[33] Single Crystal Structure Analysis Software, Version 1.6c, 1993, Molecular Structure Corporation, The Woodlands, TX, USA.
[34] M. Stähelin, D.M. Burland, J.E. Rice, Chem. Phys. Lett. 191 (1992) 245.
[35] E. Hendrickx, C. Dehu, K. Clays, J.L. Brédas, A. Persoons, in: G.A. Lindsay, K.D. Singer (Eds.), Polymers for Second-Order Nonlinear Optics, American Chemical Society, Washington, DC, 1995, p. 82.
[36] K. Clays, A. Persoons, Rev. Sci. Instrum. 63 (1992) 3285.
[37] S. Houbrechts, K. Clays, A. Persoons, Z. Pikramenou, J.-M. Lehn, Chem. Phys. Lett. 258 (1996) 485.
[38] M. Sheikh-Bahae, A.A. Said, T. Wei, D.J. Hagan, E.W. van Stryland, IEEE J. Quant. Electr. 26 (1990) 760.